



OPEN ACCESS

EDITED BY

Mona Khafaji,
Sharif University of Technology, Iran

REVIEWED BY

İskender Muz,
Nevsehir University, Türkiye
Pravin Bhattarai,
University of Galway, Ireland

*CORRESPONDENCE

Sara Mashhoun,
✉ mashhoun@kntu.ac.ir

RECEIVED 19 August 2024

ACCEPTED 16 October 2024

PUBLISHED 15 November 2024

CITATION

Mashhoun S and Tavahodi A (2024) Boron nitride nanotubes as carriers of genistein for multitherapeutic cancer treatment: A DFT study of electronic and solubility properties. *Front. Nanotechnol.* 6:1483044. doi: 10.3389/fnano.2024.1483044

COPYRIGHT

© 2024 Mashhoun and Tavahodi. This is an open-access article distributed under the terms of the [Creative Commons Attribution License \(CC BY\)](https://creativecommons.org/licenses/by/4.0/). The use, distribution or reproduction in other forums is permitted, provided the original author(s) and the copyright owner(s) are credited and that the original publication in this journal is cited, in accordance with accepted academic practice. No use, distribution or reproduction is permitted which does not comply with these terms.

Boron nitride nanotubes as carriers of genistein for multitherapeutic cancer treatment: A DFT study of electronic and solubility properties

Sara Mashhoun* and Ali Tavahodi

Department of Physics, K. N. Toosi University of Technology, Tehran, Iran

Increasing cancer mortality statistics demand more accurate and efficient treatments. Nanostructures have proved to be promising choices in this regard. Nanotubes with large surface areas can play multiple roles from drug carriers in targeted drug delivery to beam absorbers in the photothermal method. While carbon nanotubes (CNTs) show cytotoxicity, Boron Nitride Nanotubes (BNNTs) offer wide bandgap and biocompatibility. In this study, we investigate the electronic and solvation properties of (5,5), (6,6), and (7,7) BNNTs computationally by the density functional theory. For multimodal therapy, we considered Iron (Fe) doping in the BNNT, which can be helpful in hyperthermia due to the magnetic moment of Fe. Our results show that doping has improved the band positions. Furthermore, we implemented an organic anticancer molecule, genistein, a metastasis inhibitor. All potent configurations connecting genistein with BNNT covalently demonstrated enhanced water solubility as compared to pristine and Fe-doped BNNTs. The results suggest that the (7,7) C3 complex is the most stable structure and the best drug carrier.

KEYWORDS

boron nitride nanotubes (BNNTs), nanocarrier-based cancer therapy, density functional theory (DFT), genistein, doping, electronic properties, COSMO-RS

1 Introduction

Due to the inadequacy of traditional medications and treatment methods, millions of people worldwide are dying. There has always been a tradeoff between accumulating drugs in the target cell and achieving the desired distribution, solubility, and selectivity (Mortazavifar et al., 2019). There is a possibility of accumulation of drug carriers at the target site when passively targeting the pathological state of cancer cells, but effectiveness is not guaranteed. Such problems have significantly been solved by advancing drug delivery capabilities using new generations of drugs (Emanet et al., 2017; Ahmad et al., 2010). The recent development of nanocarrier-based medicines has opened a new window to a more efficient therapy method as they can be widely manipulated, resulting in greater selectivity and lower toxicity. Nanotubes are perfect nanocarrier candidates for enhancing the therapeutic effects of drugs because their wide inner and outer surface area and corresponding internal volume fundamentally open many doors for the

functionalization and even encapsulation of effective drug molecules since their endcaps can be removed (Iijima, 1991; Ferreira and Sousa, 2016).

Genistein (Gen), one of the natural and active soy isoflavones, has attracted great scientific interest due to its antitumor properties. Gen exhibits various pharmacological activities through its cancer prevention and anticancer efficacy in various preclinical model systems at low and high concentrations. Previous studies, in both *in vivo* animal tests and in human clinical trials, have shown that when consumed at low concentrations, similar to those achieved through dietary consumption, Gen inhibits the promotion of cancer cell migration, detachment, and invasion. While at high concentrations, it suppresses several proteins associated with tumorigenesis and apoptosis (Pavese et al., 2010). The broad anticancer properties of Gen include its effectiveness in inhibiting matrix metalloproteinase type 2 (MMP-2) and type 6 (MMP-6) (Huang et al., 2005; Xu et al., 2019). It also prohibits protein tyrosine kinase (PTK) and angiogenesis-promoting variables such as vascular endothelial growth factors (VEGF), which trigger the expression of the breast tumor suppressor protein BRCA. Additionally, it inhibits prostate-specific antigen (PSA) (Tyagi, Song, and De, 2019). In addition to reducing the chemoresistance and radioresistance of cancer cells, Gen is known for its antioxidant properties (Banerjee et al., 2008), which help in the treatment and control of various types of cancer, including breast cancer, prostate cancer, ovarian cancer, and colon cancer (Tyagi, Song, and De, 2019; Huang et al., 2005; Chen et al., 2020; Lee et al., 2012).

The theoretical prediction of boron nitride nanotubes (BNNTs) was made in 1994, which led to their synthesis in 1995 (Rubio et al., 1994; Blase et al., 1994). The tremendous properties of BNNTs include mechanical strength, chemical and thermal stability, electrical insulation, and biocompatibility, making them potential for numerous applications including pharmaceuticals, chemistry, high-temperature technologies, and cosmetics (Han, 2008; Lipp et al., 1989). Although they are structurally similar to carbon nanotubes (CNTs), BNNTs are considered better candidates than CNTs for various applications due to their superior properties. BNNTs are semiconductors with a wide band gap of around 5.5 eV, while CNTs can be either semiconductors or metals based on the chirality of the nanotubes (Ahmad et al., 2015). Moreover, BNNTs demonstrate higher resistance to oxidation and fewer toxic effects than CNTs in previous investigations, which makes them a preferable choice for biomedical applications (Kostoglou et al., 2020; Simon et al., 2019; Kakarla and Kong, 2022). In the context of the biological application of BNNTs, they provide promising advances in medical imaging, molecular biology, and biomedical technologies as well as theoretically supporting the identification and treatment of a range of diseases, including cancer (Ciofani et al., 2009; Ciofani et al., 2013). Although BNNTs have become a controversial figure due to their effectiveness and toxicity, many recent experimental studies suggest that they have little adverse side effects on the response of cells and organisms (Ferreira et al., 2015); for example, Chen et al. (2009) have shown that it delivers DNA into cells efficiently and without apparent toxicity.

While gold and silver nanoparticles have been studied as carriers of Gen (Ahmad et al., 2010), no research has examined BNNTs as carriers for them. When exploring a new carrier-biomaterial system,

it is wise to assess the system's properties computationally before the experimental phase to save time and money. BNNTs have diverse applications in various cancer therapy methods, including hyperthermia, boron neutron capture therapy, gene transfection, and photothermal therapy (Ferreira and Sousa, 2016). As the length of a BNNT is positively correlated with its cytotoxicity (Merlo et al., 2018), we limited the BNNT length to no more than 10 Å in this study (Kakarla and Kong, 2022; Kim et al., 2018). Doping BN nanotubes with Fe induces magnetic properties, making Fe-doped BNNTs suitable for hyperthermia and suggesting the potential of this system as an efficient drug in a multitherapeutic approach (Ciofani et al., 2009; Zhi et al., 2005). Fe can be doped in either the B-site or N-site and the magnetic moment is higher when doping a Fe atom at the B site. Doping Fe atoms in BNNTs increase their chemical reactivity compared to pure BNNTs due to their higher adsorption energy, as shown by electronic analyses. While a doped Fe atom improves adsorption performance, this atom has the greatest local reactivity and is the most reactive site. In addition to having a lower formation energy and significantly larger binding energy compared to N-site doping, the formation energy and binding energy of a Fe atom-substituted BNNT at the B site are lower, indicating a more stable structure. Among BNNTs substituted with transition metals at the B site, Fe doping achieves the shortest bond length between the doped atom and neighboring N atoms and the highest magnetic moment (Farmanzadeh and Rezaiejad, 2016; Ferreira et al., 2015; Jalalinejad et al., 2021; Li et al., 2011; Thapa et al., 2021).

2 Computational method

The study used Density Functional Theory (DFT) calculations with the Dmol3 module in Materials Studio software version 23 (Basiuk and Henao-Holguín, 2013). Dmol3 is commonly employed for various DFT calculations of transition metal-functionalized BNNTs (Zhang et al., 2012). This research focused on single-walled armchair BNNTs with three different chirality indices: (5,5), (6,6), and (7,7), which were doped with a Fe atom at the B site. These nanotubes contained 80, 96, and 112 atoms, with respective diameters of about 6.88 Å, 8.25 Å, and 9.63 Å. Additionally, the BNNTs selected had a length of approximately 7.48 Å and an average B-N bond length of 1.44 Å. Both ends were saturated with hydrogen atoms to prevent dangling bonds. The shorter length of the nanotubes provides a more favorable environment for functionalization in biomedical applications (Juárez et al., 2013).

The exchange-correlation function was estimated using the generalized gradient approximation (GGA) and the Perdew-Burke-Ernzerhof functional (PBE) (Perdew et al., 1996; Lee and Martin, 1997). GGA is preferred over local density approximation (LDA) for its more accurate estimation of interaction energies (Liang et al., 2009). For improved accuracy, unrestricted DFT with dispersion (DFT-D) developed by Grimme was employed (Delley, 2002). The DFT semi-core pseudopotentials (DSPP) with the double numerical polarization (DNP) basis set were utilized (Luo et al., 2014). The DNP basis set, available in Dmol3, is comparable to the 6-31G (d,p) and 6-31G** Gaussian basis sets and is considered one of the best basis sets (Wang et al., 2017;

Hosseinzadeh et al., 2020). The maximum energy tolerance, maximum force, and maximum displacement convergence during geometry optimization were set at 10^{-6} Ha, 0.004 Ha/Å, and 0.005Å, respectively (Warrag et al., 2020; Hatab et al., 2020; Lemaoui et al., 2021). To ensure accuracy, the multipolar expansion analysis was employed in the calculations for both gas and solution phases. For considerations in a biological context, the dielectric constant of water was used for the aqueous environment. Consequently, the conductor-like screening model for real solvation (COSMO-RS) in Dmol3 was applied for solubilization analysis (Klamt and Schüürmann, 1993).

Our proposed Gen/FeBNNT complex is formed by conjugating an active Gen molecule with the Fe atom doped in the BNNT's structure through a single covalent bond. The charge distribution, analyzed using the Hirshfeld method, and the density of states (DOSs) of the Gen/FeBNNT are discussed. To analyze the electronic properties, we calculate the energy gap (E_g) of the different configurations using E_{HOMO} and E_{LUMO} , as follows in Equation 1:

$$E_g = E_{LUMO} - E_{HOMO} \quad (1)$$

Where E_{HOMO} and E_{LUMO} represent the highest energy level of the occupied molecular orbital and the lowest energy level of the unoccupied molecular orbital, respectively.

The chemical reactivity and stability properties of the complex were investigated in both solution and gas phases by calculating the electrochemical potential (μ) (Klamt and Schüürmann, 1993), global hardness (η) (Chattaraj and Roy, 2007), and electrophilicity index (ω) (Sheela et al., 2014) as shown in Equations 2–4:

$$\mu = \frac{1}{2} (E_{LUMO} + E_{HOMO}) \quad (2)$$

$$\eta = \frac{1}{2} (E_{LUMO} - E_{HOMO}) \quad (3)$$

$$\omega = \frac{\mu^2}{2\eta} \quad (4)$$

The stability of Gen/FeBNNT complexes in the solvent model is calculated through Equation 5:

$$E_{solvation} = E_{aqueous} - E_{gas} \quad (5)$$

Where $E_{solvation}$, $E_{aqueous}$, and E_{gas} are the solvation energy of the complex, the total energy of the complex in the aqueous phase, and the total energy of the complex in the gas phase, respectively.

Equation 6 yields the adsorption energy of the optimized structure of the investigated complex (E_{ads}) as follows:

$$E_{ads} = E_{Gen/FeBNNT} - (E_{FeBNNT} + E_{Gen}) \quad (6)$$

Where $E_{Gen/FeBNNT}$ is the energy of optimized complex, E_{FeBNNT} and E_{Gen} are the energies of the BNNT doped with a Fe atom and Gen molecule, respectively.

3 Results and discussion

3.1 Geometry optimization

To gain a better understanding of how Gen interacts with FeBNNTs, we studied three different configurations for active

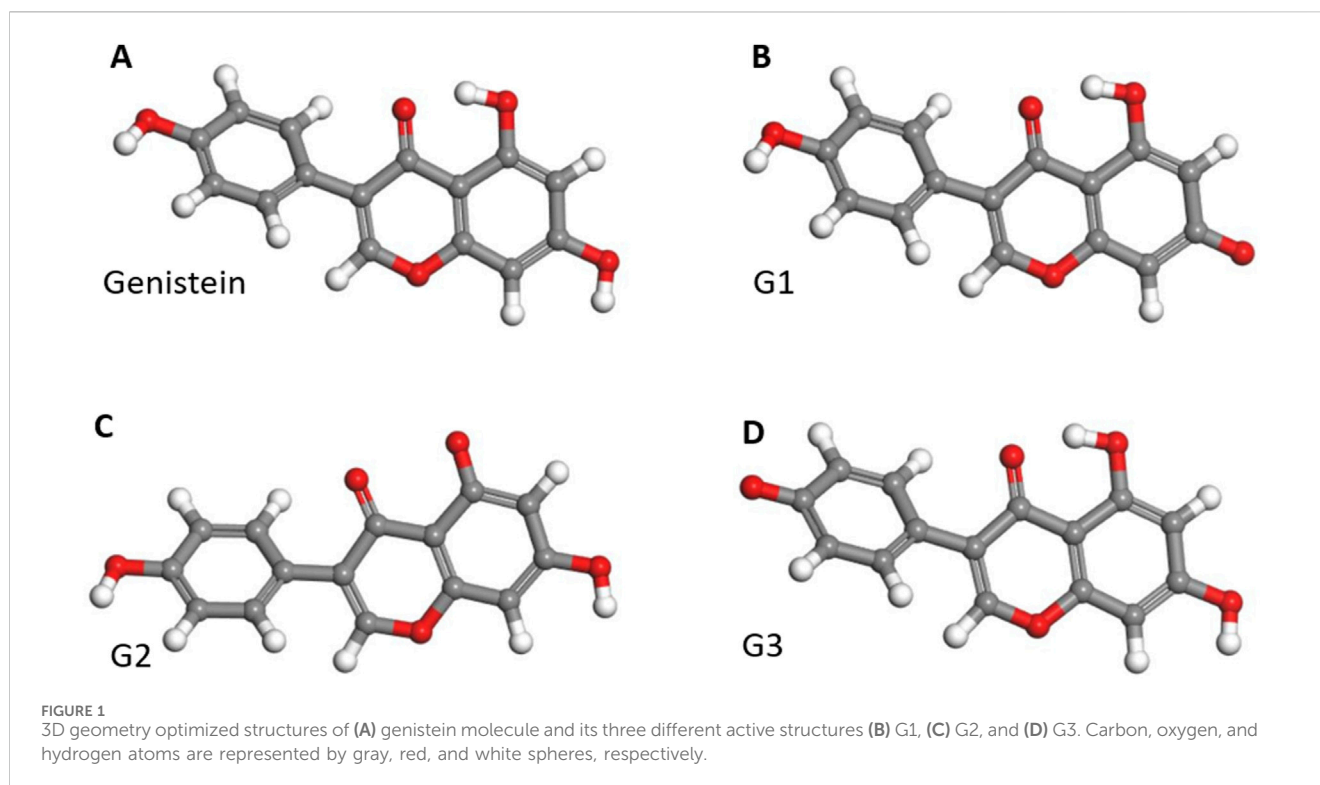
Gen molecules, named G1, G2, and G3, as depicted in Figure 1. An active Gen molecule has lost a hydrogen atom from its hydroxyl group and can form a bond with the Fe atom in the FeBNNT. Supplementary Figure S1 shows the geometrically optimized 3D structures of pristine and Fe-doped BNNTs with chiralities of (5,5), (6,6), and (7,7). The geometrically optimized 3D structures of the Gen/FeBNNT complexes can be found in Supplementary Figure S2. The complex formed by covalent bonding between the active oxygen of G1 and the Fe atom doped in the nanotube structures is labeled as C1, and so on.

Increasing the diameter of nanotubes, such as carbon nanotubes (CNTs) and aluminum nitride nanotubes (AlNNTs), can enhance the binding energy, resulting in more stable structures (Muz et al., 2021; Muz and Kurban, 2019; Muz et al., 2021). This positive correlation also applies to boron nitride nanotubes (BNNTs). Our results show that as the diameter increases from 7.16 Å to 9.98 Å, the binding energy rises from 6.56 to 6.60. Furthermore, our calculations indicate that a larger diameter can lead to a reduced energy band gap, confirming previous findings. Although the adsorption energies of C1–C3 complexes fluctuate and do not appear to be affected by diameter changes, all adsorption energies remain significantly negative, highlighting the sensing capability of BNNTs toward Gen molecules.

3.2 HOMO and LUMO analysis

Understanding the electronic properties of a molecule or complex is crucial for various applications. By analyzing the highest occupied molecular orbital (HOMO) and lowest unoccupied molecular orbital (LUMO), we can gain valuable insights into electrophilic and nucleophilic sites. Additionally, determining the HOMO and LUMO energies provides vital information about electrical transport properties by calculating the energy gap between these two levels (Shayan and Nowroozi, 2018). Supplementary Figure S3 shows the HOMO and LUMO orbitals of G1–G3, with the colors indicating the phases of the wave function (Streitwieser, 2013). Furthermore, Supplementary Figure S4 reveals the HOMO and LUMO orbitals of pristine and Fe-doped BNNTs, showing the localized HOMO orbitals around nitrogen atoms in pristine BNNTs and the strong localization of the LUMO orbitals around the Fe atom in FeBNNTs. Thus, Fe atoms in the doped nanotubes are susceptible to nucleophilic attack (Xu et al., 2018). Meanwhile, Supplementary Figure S3 indicates that the HOMO orbitals are located at the active oxygen in the G1–G3 structures. Our results suggest that the interaction between the active oxygen site in Gen and the Fe atom doped in the nanotube is very likely, facilitating the formation of the C1–C3 Gen-nanotube complexes we offer. According to Supplementary Figures S5–S7, the HOMO and LUMO of the C1 complexes in all nanotubes considered show charge transfer from the HOMO to the LUMO since they are located on the Gen molecule and the Fe-doped nanotubes, respectively.

Using the HOMO and LUMO orbital energies, we can calculate the electrochemical potential (μ), global hardness (η), and electrophilicity index (ω). In the gas phase, a distinct interaction between Gen and BNNT is observed without external effects, whereas in the aqueous solution phase, the solvent has a



noticeable impact on the energetic interaction between Gen and the nanotube in a biological system (Bououden et al., 2021).

Supplementary Tables S1, S2 present the results of the electronic property calculations for the C1-C3 complexes in both gas and solution phases. When a Fe atom is doped into the BNNT structures, the energy gap, indicated by $|E_{LUMO} - E_{HOMO}|$, is significantly reduced. This reduction follows the same order as the global hardness in all C1-C3 complexes, in both phases:

C2 configurations < C1 configurations < C3 configurations.

This result illustrates that C2 configurations exhibit the highest chemical reactivity and the lowest kinetic stability, in contrast to C3 configurations, which demonstrate the lowest chemical reactivity and the highest kinetic stability. However, the reduction in E_g after the Gen/nanotube interaction shows successful charge transfer from donor to acceptor and better bonding (Shayan and Nowroozi, 2018). In Supplementary Table S1, it is shown that after the complex is formed, the bandgap (E_g) is reduced to around 1eV. This reduction in bandgap causes longer excitation wavelengths in the red and infrared regions, which makes the proposed complexes suitable for the photothermal method. The quantitative calculations for the excitation wavelength of the complex can be found in the Supplementary Material. When a Fe atom is doped at the B site of the pristine BNNT and the Gen molecule is adsorbed on it, the global hardness decreases by about 1.7 eV and the gap energy decreases by about 3 eV. The exception is observed in the C2 configuration of (5,5) and (6,6) BNNTs in the gas phase, where the energy gap decreases by approximately 4 eV.

In both phases, the chemical potential of all considered Fe-doped nanotubes decreases by about 0.5 eV compared to their pristine nanotubes, except for (5,5) FeBNNT in the gas phase, which is reduced by about 1 eV, possibly due to the morphological properties of the nanotube. This indicates

increased reactivity by doping a Fe atom as well as improved adsorption.

Charge transfer can occur from a higher chemical potential to a lower one (Kamel et al., 2018). It is worth noting that the chemical potential of C1-C3 complexes in the gas and solution phases varies in the range of about -4.3 eV to -4.8 eV.

Lower chemical potential in the solution phase may be due to solvation effects and increased entropy, resulting in a more stable and favorable structure. The electrophilicity index values of C1-C3 complexes are at least about six times higher than those of pristine nanotubes in both phases. A higher electrophilicity index reflects higher stability of the complex.

Among all complexes considered, (6,6) C2 and (6,6) C3 have the highest and the lowest electrophilicity index in the gas phase, respectively, while (6,6) C1 and (7,7) C3 in the solution phase have the highest and the lowest electrophilicity index, respectively.

Supplementary Table S2 shows the same DFT calculation in the Dmol3 module performed for the solution phase to study the behavior of Gen/FeBNNT complexes in the human body. Water with a dielectric constant of 78.54 was used as the solvent to simulate the human biological system best. A comparison with the gas phase revealed that the band gap energy of (5,5) C2 and (6,6) C2 complexes in the solution phase increased by approximately 0.7 and 0.9 eV, respectively. For other complexes, these fluctuations were less than about 0.15 eV. In the solution phase, the electrophilicity index for (5,5) C2 and (6,6) C2 complexes decreased by almost half, while it increased for all other complexes compared to the gas phase. Additionally, the Fe-O bond length between Gen and nanotube decreased by about 0.1 Å in the mentioned structures. Fluctuations in the electrophilicity index in the solution phase, compared to the gas phase, could have various causes, such as changes in the activity coefficients of the reactants in different reaction pathways.

TABLE 1 Calculated E_{ads} in the gas phase and solution phase and $E_{solvation}$ for studied complexes.

System	E_{ads} (gas phase) (kJ/mol)	E_{ads} (solution phase) (kJ/mol)	$E_{solvation}$ (kJ/mol)
(5,5) C1	-348.958	-283.515	-157.598
(5,5) C2	-402.584	-277.857	-123.162
(5,5) C3	-351.294	-256.637	-128.649
(6,6) C1	-370.721	-251.890	-137.122
(6,6) C2	-411.833	-260.764	-129.739
(6,6) C3	-358.021	-247.873	-147.582
(7,7) C1	-381.012	-275.743	-158.170
(7,7) C2	-385.371	-263.204	-166.131
(7,7) C3	-361.321	-252.342	-156.246

Table 1 lists the adsorption energy of a Gen molecule to BNNTs with C1-C3 configurations in both the solution and gas phases, as well as the solvation energy of the studied complexes, calculated by Equations 5, 6. Negative values indicate that the interaction between the Gen molecule and the Fe-doped BNNT is an exothermic reaction, suggesting more stable interactions. The fluctuations in adsorption energy between the gas phase and the solution phase (e.g. water) are due to solvation effects (Chen and Wu, 1998; Singh and Campbell, 2019). The C2 configurations have the highest absolute value of adsorption energy in all phases except for the (5,5) and (7,7) configurations in the solution phase, where their C1 configurations have a slightly higher absolute value than their C2 complexes. However, the C3 complexes have the lowest absolute value overall, yet remain advantageous. Additionally, the solvation energy values are negative, indicating that the solvation of the studied complexes in water occurs spontaneously and therefore they are readily soluble in water. This is advantageous for their use in a biological system. The (7,7) complexes generally have higher solvation energy compared to other complexes, and one of the reasons for this is their higher electrostatic interactions (Wei and Luo, 2018).

Based on the information in Supplementary Table S3, which displays the order of the C1-C3 complexes in terms of, E_g , μ , η , ω , E_{ads} , $E_{solvation}$, we can infer that the (7,7) C3 Gen-FeBNNT complex offers the highest stability and one of the best solubilities in water. As a result, it is considered the top candidate for use in biological systems.

3.3 Density of states (DOS)

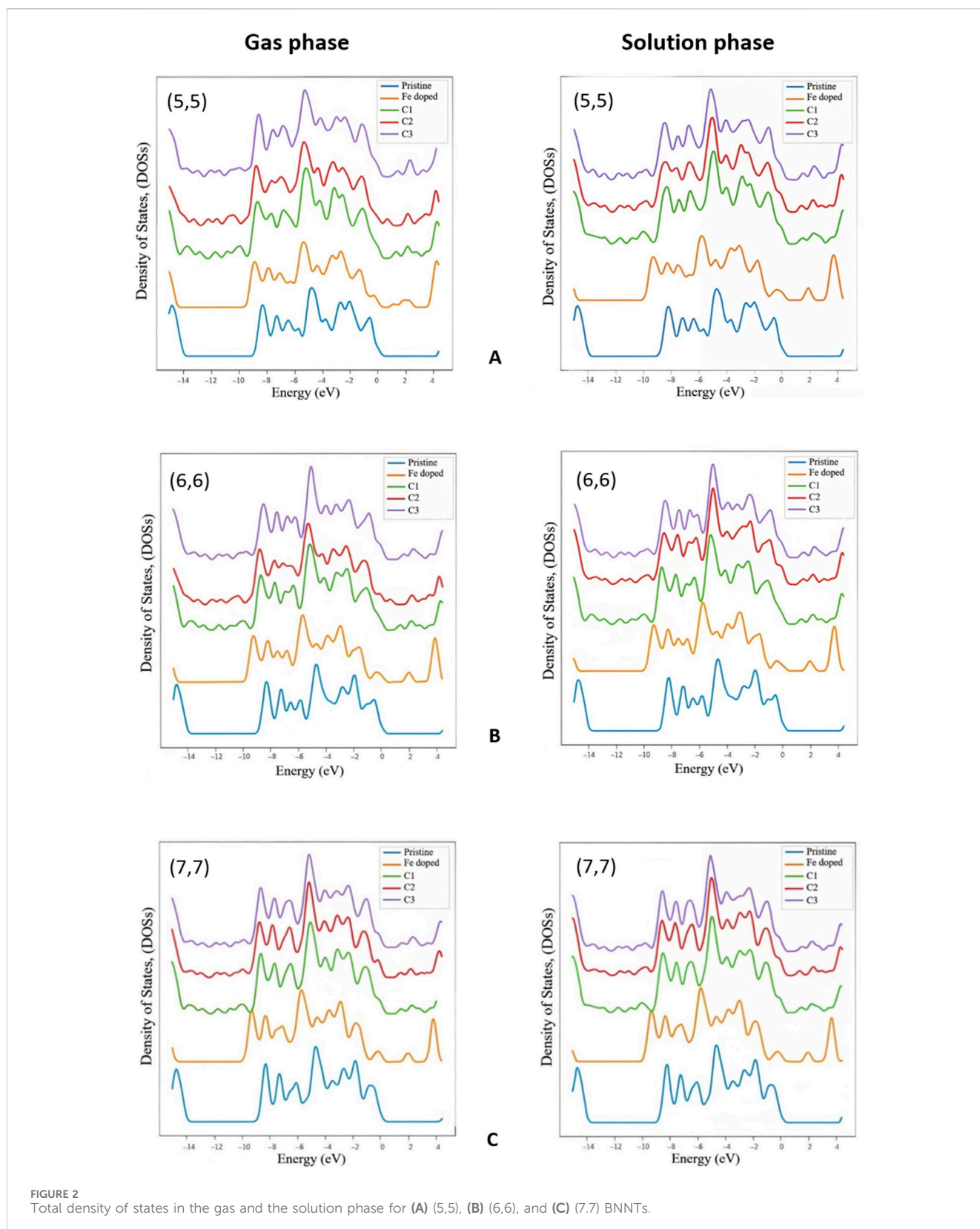
To understand the effects of the Gen molecule adsorption on the electronic properties of the studied nanotubes, we calculated the total density of states (DOSs). The results are shown in Figure 2, which shows the DOS of the pristine BNNT, the Fe-doped BNNT, and the C1-C3 complexes. BNNTs are semiconductors with a wide band gap of about 5 eV, achieved by HOMO-LUMO gap, tight binding, or ab initio-based calculations, and our determined energy gaps for studied pristine nanotubes are consistent with previous works (Wu, Yang, and Zeng, 2006; Bououden et al., 2021; Hosseinzadeh et al., 2020). Doping a Fe atom into these

structures significantly reduced the energy band gap to generally around 1.9 eV, increased the valence bandwidth and added a peak at the top of this band. The highest peak in the valence band varies about 1 eV, which is generally around -5.7 eV for doped nanotubes in all phases (except for the (5,5) chirality in the gas phase, which is at -5.35 eV in the doped state and differs from their pristine model by 0.5 eV). The mentioned peak appeared to be at around 0.7 eV higher level after the Gen molecule interaction, except for the (5,5) chirality in the gas phase, which remains almost the same. As we can see Gen molecule's covalent bonding with the Fe atom in BNNT structures slightly decreases the energy gap compared to the Fe-doped structures. As a result, the studied Fe-doped BNNTs offer higher conductivity in the range of 0-4 eV when functionalized with a Gen molecule, demonstrating their reduced semiconductor behavior and improved electronic properties.

3.4 Sigma profiles and COSMO 3D surfaces

When conducting DFT calculations using the Dmol3 module for aqueous phases, we utilized COSMO-RS to generate sigma profiles and COSMO 3D surfaces for the molecules and complexes under investigation. The sigma profile is a distribution function that illustrates the average screening charge density on specific segments of a molecule or complex (Mohammed et al., 2023; Babiker, Shuhaimi, and Mutalib, 2014). Supplementary Figures S8, S9 display the COSMO surfaces of active Gen molecules and pristine and doped BNNTs. The COSMO surfaces of various BNNT complexes are shown in Supplementary Figures S10-S12. Additionally, Supplementary Figure S13 presents sigma profiles, which are categorized into three segments as follows:

- Sigma profile values less than -0.01 indicate positive charges and hydrogen bond donor (HBD) regions, displayed as red segments on the COSMO surface.
- Sigma profile values greater than +0.01 represent negative charges and hydrogen bond acceptor (HBA) regions, shown as blue segments on the COSMO surface.
- Sigma profile values between -0.01 and +0.01 signify neutral charges and non-polar regions of the COSMO surface (Boudjelida et al., 2022).



In [Supplementary Figure S13](#), we observe at least three peaks in the HBD regions for all G1-G3 molecules. The COSMO surfaces in [Supplementary Figure S8](#) display these regions in red color, indicating the presence of active oxygen molecules. Both pristine

and Fe-doped BNNTs do not reach the HBA region. However, when interacting with G1-G3, a very weak peak appears. There is a weak peak in the HBD region for all studied pristine BNNTs, while this peak is slightly higher and broader for C1-C3 complexes. The

equilibrium between HBD and HBA peaks of the C1–C3 complexes, caused by the presence of oxygen and hydrogen atoms in the Gen molecule, suggests better solvation and increased hydrophilic behavior (Hosseini et al., 2019). In the non-polar area, the Gen-nanotube complexes display a higher and broader peak compared to the pristine BNNTs, with the C3 configuration showing the highest peak except in (5,5) chirality, where the C2 complex has the highest peak. This indicates better dispersion in water for these complexes.

4 Conclusion

In the present study, we have proposed a new complex involving boron nitride nanotubes and a biomolecule for treating cancer through multiple methods. We used DFT calculations to study boron nitride nanotubes with armchair structure and chirality indices of (5,5), (6,6), and (7,7). These nanotubes act as carriers for the anti-cancer biomolecule, genistein. We also studied the effects of introducing iron (Fe) into the nanotubes, which enhanced their electronic and magnetic properties and facilitated bonding with the genistein molecule. We investigated three different configurations of covalent bonding between the active oxygen in genistein and the doped Fe atom, labeled C1, C2, and C3. We examined the proposed complexes in both solution and gas phase. Our findings indicated that the adsorption of genistein on the nanotube surface led to a reduction in the band gap. This reduction subsequently led to a higher excitation wavelength in the infrared region, pointing to the exceptional potential of the complex for photothermal treatment. Moreover, the inclusion of Fe resulted in the addition of a magnetic moment to the structure, potentially reducing the necessary magnetic field application to the human body in hyperthermia treatment and enabling more precise cell targeting. Notably, the studied complex also presents a significant advantage in providing an adequate dose of boron atoms for boron neutron capture therapy, underscoring its potential as a multi-therapeutic treatment.

The comprehensive analysis of the quantum molecular descriptors of the complexes revealed that the (7, 7) C3 and (6, 6) C3 configurations exhibited the greatest stability and the least chemical reactivity in both phases. All interactions were found to be exothermic and stable, with high adsorption energy values for the mentioned complexes. The solvation energy comparison showed that (7, 7) genistein-nanotube complexes were the most soluble structures. The total density of states (DOS) of the complexes displayed a reduction in the band gap after the interaction, which is in agreement with the energy gap values calculated by the highest occupied molecular orbital (HOMO) and lowest unoccupied molecular orbital (LUMO). The sigma profile from COSMO-RS files showed that the hydrophilic behavior and dispersion of the complexes in water were enhanced after interaction with genistein molecules.

References

Ahmad, M. Z., Akhter, S., Jain, G. K., Rahman, M., Ahmad Pathan, S., Ahmad, F. J., et al. (2010). Metallic nanoparticles: technology overview and drug delivery applications in oncology. *Expert Opin. drug Deliv.* 7 (8), 927–942. doi:10.1517/17425247.2010.498473

Ultimately, the rigorous analysis led to the unequivocal conclusion that the (7, 7) C3 complex emerges as the optimal genistein carrier within the biological system. Further experimental investigations are encouraged to synthesize and characterize the proposed complex.

Data availability statement

The original contributions presented in the study are included in the article/[Supplementary Material](#), further inquiries can be directed to the corresponding author.

Author contributions

SM: Conceptualization, Investigation, Visualization, Writing–original draft, Writing–review and editing, Project administration, Supervision. AT: Conceptualization, Investigation, Visualization, Writing–original draft, Writing–review and editing, Data curation, Software.

Funding

The author(s) declare that no financial support was received for the research, authorship, and/or publication of this article.

Conflict of interest

The authors declare that the research was conducted in the absence of any commercial or financial relationships that could be construed as a potential conflict of interest.

Publisher's note

All claims expressed in this article are solely those of the authors and do not necessarily represent those of their affiliated organizations, or those of the publisher, the editors and the reviewers. Any product that may be evaluated in this article, or claim that may be made by its manufacturer, is not guaranteed or endorsed by the publisher.

Supplementary material

The Supplementary Material for this article can be found online at: <https://www.frontiersin.org/articles/10.3389/fnano.2024.1483044/full#supplementary-material>

Ahmad, P., Uddin Khandaker, M., Khan, Z. R., and Amin, Y. M. (2015). Synthesis of boron nitride nanotubes via chemical vapour deposition: a comprehensive review. *RSC Adv.* 5 (44), 35116–35137. doi:10.1039/c5ra01594d

- Babiker, O. E., Shuhaimi, M., and Mutalib, M. I. A. (2014). Molecular simulation for piperazinium based ILs: effects of alkyl chain, concentration and anions on Henry's constants. *Appl. Mech. Mater.* 625, 448–453. doi:10.4028/www.scientific.net/amm.625.448
- Banerjee, S., Li, Y., Wang, Z., and Sarkar, F. H. (2008). Multi-targeted therapy of cancer by genistein. *Cancer Lett.* 269 (2), 226–242. doi:10.1016/j.canlet.2008.03.052
- Basiuk, V. A., and Hena-Holguín, L. V. (2013). Effects of orbital cutoff in DMol3 DFT calculations: a case study of meso-tetraphenylporphyrin-C60 complex. *J. Comput. Theor. Nanosci.* 10 (5), 1266–1272. doi:10.1166/jctn.2013.2840
- Blase, X., Rubio, A., Louie, S. G., and Cohen, M. L. (1994). Stability and band gap constancy of boron nitride nanotubes. *Europhys. Lett.* 28 (5), 335–340. doi:10.1209/0295-5075/28/5/007
- Boudjelida, S., Djellali, S., Ferkous, H., Benguerba, Y., Chikouche, I., and Carraro, M. (2022). Physicochemical properties and atomic-scale interactions in polyaniline (Emeraldine Base)/starch bio-based composites: experimental and computational investigations. *Polymers* 14 (8), 1505. doi:10.3390/polym14081505
- Bououden, W., Benguerba, Y., Darwish, A. S., Attoui, A., Lemaoui, T., Balsamo, M., et al. (2021). Surface adsorption of Crizotinib on carbon and boron nitride nanotubes as Anti-Cancer drug Carriers: COSMO-RS and DFT molecular insights. *J. Mol. Liq.* 338, 116666. doi:10.1016/j.molliq.2021.116666
- Chattaraj, P. K., and Roy, D. R. (2007). Update 1 of: electrophilicity index. *Chem. Rev.* 107 (9), PR46–PR74. doi:10.1021/cr078014b
- Chen, C.-yu, and Wu, S.-chee (1998). The influence of relative humidity on the adsorption of toluene by soils—interpretation with the adsorption energy distribution functions. *Chemosphere* 37 (8), 1437–1444. doi:10.1016/s0045-6535(98)00134-9
- Chen, X., Wu, P., Rouseas, M., Okawa, D., Gartner, Z., Zettl, A., et al. (2009). Boron nitride nanotubes are noncytotoxic and can be functionalized for interaction with proteins and cells. *J. Am. Chem. Soc.* 131 (3), 890–891. doi:10.1021/ja807334b
- Chen, X., Wu, Y., Gu, J., Liang, P., Shen, M., Xi, J., et al. (2020). Anti-invasive effect and pharmacological mechanism of genistein against colorectal cancer. *Biofactors* 46 (4), 620–628. doi:10.1002/biof.1627
- Ciofani, G., Danti, S., Graziana Genchi, G., Mazzolai, B., and Mattoli, V. (2013). Boron nitride nanotubes: biocompatibility and potential spill-over in nanomedicine. *Small* 9 (9–10), 1672–1685. doi:10.1002/sml.201201315
- Ciofani, G., Raffa, V., Mencias, A., and Cuschieri, A. (2009). Boron nitride nanotubes: an innovative tool for nanomedicine. *Nano Today* 4 (1), 8–10. doi:10.1016/j.nantod.2008.09.001
- Ciofani, G., Raffa, V., Yu, J., Chen, Y., Obata, Y., Takeoka, S., et al. (2009). Boron nitride nanotubes: a novel vector for targeted magnetic drug delivery. *Curr. Nanosci.* 5 (1), 33–38. doi:10.2174/157341309787314557
- Delley, B. (2002). Hardness conserving semilocal pseudopotentials. *Phys. Rev. B* 66 (15), 155125. doi:10.1103/physrevb.66.155125
- Emanet, M., Şen, Ö., and Çulha, M. (2017). Evaluation of boron nitride nanotubes and hexagonal boron nitrides as nanocarriers for cancer drugs. *Nanomedicine* 12 (7), 797–810. doi:10.2217/nmm-2016-0322
- Farmanzadeh, D., and Rezaei, H. (2016). Adsorption of diazinon and hinosan molecules on the iron-doped boron nitride nanotubes surface in gas phase and aqueous solution: a computational study. *Appl. Surf. Sci.* 364, 862–869. doi:10.1016/j.apsusc.2015.12.202
- Ferreira, T. H., Marino, A., Rocca, A., Liakos, I., Nitti, S., Athanassiou, A., et al. (2015). Folate-grafted boron nitride nanotubes: possible exploitation in cancer therapy. *Int. J. Pharm.* 481 (1–2), 56–63. doi:10.1016/j.ijpharm.2015.01.048
- Ferreira, T. H., Silva, PROD, Santos, R. G. D., and Sousa, E. M. (2011). A novel synthesis route to produce boron nitride nanotubes for bioapplications. *J. Biomater. Nanobiotechnology* 2 (04), 426–434. doi:10.4236/jbnt.2011.24052
- Ferreira, T. H., and Sousa, E. M. B. de (2016). “Applications and perspectives of boron nitride nanotubes in cancer therapy,” in *Boron nitride nanotubes in nanomedicine* (Elsevier), 95–109.
- Han, W.-Q. (2009). “Anisotropic Hexagonal Boron Nitride Nanomaterials: Synthesis and Applications,” in *Nanotechnologies for the Life Sciences* (Wiley). doi:10.1002/9783527610419.nts0161
- Hatab, F. A., Darwish, A. S., Lemaoui, T., Warrag, S. E. E., Benguerba, Y., Kroon, M. C., et al. (2020). Extraction of thiophene, pyridine, and toluene from n-decane as a diesel model using betaine-based natural deep eutectic solvents. *J. Chem. and Eng. Data* 65 (11), 5443–5457. doi:10.1021/acs.jced.0c00579
- Hosseini, E., Zakertabrizi, M., Korayem, A. H., and Shahsavari, R. (2019). Tunable, multifunctional ceramic composites via intercalation of fused graphene boron nitride nanosheets. *ACS Appl. Mater. and Interfaces* 11 (8), 8635–8644. doi:10.1021/acsami.8b19409
- Hosseinzadeh, B., Beni, A. S., Eskandari, R., Karami, M., and Khorram, M. (2020). Interaction of propylthiouracil, an anti-thyroid drug with boron nitride nanotube: a DFT study. *Adsorption* 26, 1385–1396. doi:10.1007/s10450-020-00248-x
- Huang, X., Chen, S., Xu, L., Liu, Y., Deb, D. K., Platanius, L. C., et al. (2005). Genistein inhibits p38 map kinase activation, matrix metalloproteinase type 2, and cell invasion in human prostate epithelial cells. *Cancer Res.* 65 (8), 3470–3478. doi:10.1158/0008-5472.can-04-2807
- Iijima, S. (1991). Helical microtubules of graphitic carbon. *nature* 354 (6348), 56–58. doi:10.1038/354056a0
- Jalalinejad, A., Yeganeg, M., Farokhzad, M., Bagheri, M., Bahari, A., and Gholizadeh, A. (2021). Structural, magnetic, and electronic properties and stability of 3d-TM substituted single-walled zigzag BNNTs: a density functional theory study. *Comput. Condens. Matter* 28, e00575. doi:10.1016/j.cocom.2021.e00575
- Juárez, A. R., Chigo Anota, E., Cocolletzi, H. H., and Riveros, A. F. (2013). Adsorption of chitosan on BN nanotubes: a DFT investigation. *Appl. Surf. Sci.* 268, 259–264. doi:10.1016/j.apsusc.2012.12.075
- Kakarla, A. B., and Kong, I. (2022). *In vitro* and *in vivo* cytotoxicity of boron nitride nanotubes: a systematic review. *Nanomaterials* 12 (12), 2069. doi:10.3390/nano12122069
- Kamel, M., Raissi, H., Ali, M., and Shahabi, M. (2018). Assessment of the adsorption mechanism of Flutamide anticancer drug on the functionalized single-walled carbon nanotube surface as a drug delivery vehicle: an alternative theoretical approach based on DFT and MD. *Appl. Surf. Sci.* 434, 492–503. doi:10.1016/j.apsusc.2017.10.165
- Kim, J. H., Pham, T. V., Hwang, J. H., Kim, C. S., and Kim, M. J. (2018). Boron nitride nanotubes: synthesis and applications. *Nano Conver.* 5 (1), 17. doi:10.1186/s40580-018-0149-y
- Klamt, A., and Schüürmann, GJGJ (1993). COSMO: a new approach to dielectric screening in solvents with explicit expressions for the screening energy and its gradient. *J. Chem. Soc. Perkin Trans.* 2 (5), 799–805. doi:10.1039/p29930000799
- Kostoglou, N., Tampaxis, C., Charalambopoulou, G., Constantinides, G., Ryzhkov, V., Doumanidis, C., et al. (2020). Boron nitride nanotubes versus carbon nanotubes: a thermal stability and oxidation behavior study. *Nanomater. (Basel)* 10 (12), 2435. doi:10.3390/nano10122435
- Lee, I.-Ho, and Martin, R. M. (1997). Applications of the generalized-gradient approximation to atoms, clusters, and solids. *Phys. Rev. B* 56 (12), 7197–7205. doi:10.1103/physrevb.56.7197
- Lee, J.-Y., Kim, H. S., and Song, Y.-S. (2012). Genistein as a potential anticancer agent against ovarian cancer. *J. Traditional Complementary Med.* 2 (2), 96–104. doi:10.1016/s2225-4110(16)30082-7
- Lemaoui, T., Benguerba, Y., Darwish, A. S., Hatab, F. A., Warrag, S. E. E., Kroon, M. C., et al. (2021). Simultaneous dearomatization, desulfurization, and denitrogenation of diesel fuels using acidic deep eutectic solvents as extractive agents: a parametric study. *Sep. Purif. Technol.* 256, 117861. doi:10.1016/j.seppur.2020.117861
- Li, X.-M., Tian, W. Q., Qi, D., Huang, X.-Ri, Sun, C.-C., and Jiang, L. (2011). Substitutional doping of BN nanotube by transition metal: a density functional theory simulation. *Comput. Theor. Chem.* 964 (1–3), 199–206. doi:10.1016/j.comptc.2010.12.026
- Liang, T., Li, W.-X., and Zhang, H. (2009). A first-principles study on the behavior of HCl inside SWCNT. *J. Mol. Struct. THEOCHEM* 905 (1–3), 44–47. doi:10.1016/j.theochem.2009.03.007
- Lipp, A., Schwetz, K. A., and Hunold, K. (1989). Hexagonal boron nitride: fabrication, properties and applications. *J. Eur. Ceram. Soc.* 5 (1), 3–9. doi:10.1016/0955-2219(89)90003-4
- Luo, Y., Yin, S., Lai, W., and Wang, Y. (2014). Effects of global orbital cutoff value and numerical basis set size on accuracies of theoretical atomization energies. *Theor. Chem. Accounts* 133, 1–11. doi:10.1007/s00214-014-1580-8
- Merlo, A., Mokkaipati, V. R. S. S., Pandit, S., and Mijakovic, I. (2018). Boron nitride nanomaterials: biocompatibility and bio-applications. *Biomater. Sci.* 6 (9), 2298–2311. doi:10.1039/C8BM00516H
- Mohammed, S. A. S., Yahya, W. Z. N., Bustam, M. A., and Kibria, Md G. (2023). Experimental and computational evaluation of 1, 2, 4-triazolium-based ionic liquids for carbon dioxide capture. *Separations* 10 (3), 192. doi:10.3390/separations10030192
- Mortazavifar, A., Raissi, H., and Akbari, A. (2019). DFT and MD investigations on the functionalized boron nitride nanotube as an effective drug delivery carrier for Carmustine anticancer drug. *J. Mol. Liq.* 276, 577–587. doi:10.1016/j.molliq.2018.12.028
- Muz, Í., Alaei, S., and Kurban, M. (2021). Sensing capability and diameter-dependent electronic structure of boron nitride nanotubes. *Mater. Today Commun.* 27, 102252. doi:10.1016/j.mtcomm.2021.102252
- Muz, Í., Kurban, H., and Kurban, M. (2021). A DFT study on stability and electronic structure of AlN nanotubes. *Mater. Today Commun.* 26, 102118. doi:10.1016/j.mtcomm.2021.102118
- Muz, I., and Kurban, M. (2019). A comprehensive study on electronic structure and optical properties of carbon nanotubes with doped B, Al, Ga, Si, Ge, N, P and as and different diameters. *J. Alloys Compd.* 802, 25–35. doi:10.1016/j.jallcom.2019.06.210
- Pavese, J. M., Farmer, R. L., and Bergan, R. C. (2010). Inhibition of cancer cell invasion and metastasis by genistein. *Cancer Metastasis Rev.* 29, 465–482. doi:10.1007/s10555-010-9238-z
- Perdew, J. P., Burke, K., and Ernzerhof, M. (1996). Generalized gradient approximation made simple. *Phys. Rev. Lett.* 77 (18), 3865–3868. doi:10.1103/physrevlett.77.3865

- Rubio, A., Corkill, J. L., and Cohen, M. L. (1994). Theory of graphitic boron nitride nanotubes. *Phys. Rev. B* 49 (7), 5081–5084. doi:10.1103/physrevb.49.5081
- Shayan, K., and Nowroozi, A. (2018). Boron nitride nanotubes for delivery of 5-fluorouracil as anticancer drug: a theoretical study. *Appl. Surf. Sci.* 428, 500–513. doi:10.1016/j.apsusc.2017.09.121
- Sheela, N. R., Muthu, S., and Sampathkrishnan, S. (2014). Molecular orbital studies (hardness, chemical potential and electrophilicity), vibrational investigation and theoretical NBO analysis of 4-4'-(1H-1, 2, 4-triazol-1-yl methylene) dibenzonitrile based on abinitio and DFT methods. *Spectrochimica Acta Part A Mol. Biomol. Spectrosc.* 120, 237–251. doi:10.1016/j.saa.2013.10.007
- Simon, J., Flahaut, E., and Golzio, M. (2019). Overview of carbon nanotubes for biomedical applications. *Mater. (Basel)* 12 (4), 624. doi:10.3390/ma12040624
- Singh, N., and Campbell, C. T. (2019). A simple bond-additivity model explains large decreases in heats of adsorption in solvents versus gas phase: a case study with phenol on Pt (111) in water. *ACS Catal.* 9 (9), 8116–8127. doi:10.1021/acscatal.9b01870
- Streitwieser, A. (2013). Molecular orbital theory for organic chemists in pioneers of quantum chemistry, in *ACS symposium series* (American Chemical Society), 275–300.
- Thapa, A., Chettri, B., Sarkar, A., Chandra Pradhan, P., and Sharma, B. (2021). Computational analysis and first principle study of electrical and optical properties of Fe doped SWBNNT and its application.
- Tyagi, N., Song, Yo H., and De, R. (2019). Recent progress on biocompatible nanocarrier-based genistein delivery systems in cancer therapy. *J. Drug Target.* 27 (4), 394–407. doi:10.1080/1061186x.2018.1514040
- Wang, R., Zhang, D., and Liu, C. (2017). DFT study of the adsorption of 2, 3, 7, 8-tetrachlorodibenzo-p-dioxin on pristine and Ni-doped boron nitride nanotubes. *Chemosphere* 168, 18–24. doi:10.1016/j.chemosphere.2016.10.050
- Warrag, S. E. E., Darwish, A. S., Abuhatab, F. O. S., Adeyemi, I. A., Kroon, M. C., and AlNashef, I. M. (2020). Combined extractive dearomatization, desulfurization, and denitrogenation of oil fuels using deep eutectic solvents: a parametric study. *Industrial and Eng. Chem. Res.* 59 (25), 11723–11733. doi:10.1021/acs.iecr.0c01360
- Wei, X., and Luo, T. (2018). Effects of electrostatic interaction and chirality on the friction coefficient of water flow inside single-walled carbon nanotubes and boron nitride nanotubes. *J. Phys. Chem. C* 122 (9), 5131–5140. doi:10.1021/acs.jpcc.7b11657
- Wu, X., Yang, J. L., and Zeng, X. C. (2006). Adsorption of hydrogen molecules on the platinum-doped boron nitride nanotubes. *J. Chem. Phys.* 125 (4), 44704. doi:10.1063/1.2210933
- Xu, H., Li, L., Fan, G., and Chu, X. (2018). DFT study of nanotubes as the drug delivery vehicles of Efavirenz. *Comput. Theor. Chem.* 1131, 57–68. doi:10.1016/j.comptc.2018.03.032
- Xu, Li, Liu, J.-tian, Li, K., Wang, S.-yu, and Xu, S. (2019). Genistein inhibits Ang II-induced CRP and MMP-9 generations via the ER-p38/ERK1/2-PPAR γ -NF- κ B signaling pathway in rat vascular smooth muscle cells. *Life Sci.* 216, 140–146. doi:10.1016/j.lfs.2018.11.036
- Zhang, Z.-W., Zheng, W.-T., and Jiang, Q. (2012). Hydrogen adsorption on Ce/BNNT systems: A DFT study. *Int. J. Hydrogen Energy.* 37 (6), 5090–5099. doi:10.1016/j.ijhydene.2011.12.036
- Zhi, C., Bando, Y., Tang, C., Golberg, D., Xie, R., and Sekigushi, T. (2005). Phonon characteristics and cathodoluminescence of boron nitride nanotubes. *Appl. Phys. Lett.* 86 (21). doi:10.1063/1.1938002